COMPARATIVE ANALYSIS OF MOLECULAR CLOUDS IN M31, M33, AND THE MILKY WAY

Kartik Sheth

Spitzer Science Center, California Institute of Technology, MS 105-24, Pasadena, CA 91125; kartik@astro.caltech.edu

Stuart N. Vogel

Department of Astronomy, University of Maryland, College Park, MD 20742-2421; vogel@astro.umd.edu

Christine D. Wilson

Department of Physics and Astronomy, McMaster University, Hamilton, ON L8S 4M1, Canada; wilson@physics.mcmaster.ca

and

T. M. Dame

Harvard-Smithsonian Center for Astrophysics, Mail Stop 72, 60 Garden Street, Cambridge, MA 02138; tdame@cfa.harvard.edu

ABSTRACT

We present BIMA observations of a $2'$ field in the northeastern spiral arm of M31. In this region we find six giant molecular clouds (GMCs) that have a mean diameter of 57 ± 13 pc, a mean velocity width of 6.5 ± 1.2 km s^{-1}, and a mean molecular mass of $(3.0 \pm 1.6) \times 10^5 \ M_\odot$. The peak brightness temperature of these clouds ranges from 1.6 to 4.2 K. We compare these clouds to clouds in M33 observed by Wilson & Scoville using the OVRO millimeter array and some cloud complexes in the Milky Way observed by Dame and coworkers using the CfA 1.2 m telescope. In order to properly compare the single-dish data to the spatially filtered interferometric data, we project several well-known Milky Way complexes to the distance of Andromeda and simulate their observation with the BIMA interferometer. We compare the simulated Milky Way clouds with the M31 and M33 data using the same cloud identification and analysis technique and find no significant differences in the cloud properties in all three galaxies. Thus, we conclude that previous claims of differences in the molecular cloud properties between these galaxies may have been due to differences in the choice of cloud identification techniques. With the upcoming CARMA telescope, individual molecular clouds may be studied in a variety of nearby galaxies. With ALMA, comprehensive GMC studies will be feasible at least as far as the Virgo cluster. With these data, comparative studies of molecular clouds across galactic disks of all types and between different galaxy disks will be possible. Our results emphasize that interferometric observations combined with the use of a consistent cloud identification and analysis technique will be essential for such forthcoming studies that will compare GMCs in the Local Group galaxies to galaxies in the Virgo cluster.

Subject headings: galaxies: individual (M31, M33, Milky Way) — galaxies: ISM — Local Group — radio lines: ISM

Online material: color figure

1. INTRODUCTION

In the inner disk of the Milky Way, the dominant component of the interstellar medium (ISM) is molecular gas, which is distributed in discrete cloud complexes (Scoville et al. 1987; Scoville 1990). Nearly all star formation in our Galaxy is associated with these clouds (Scoville et al. 1987; Blitz 1993). Therefore, understanding the distribution and properties of molecular clouds is a prerequisite for understanding galaxy evolution. Studies of the molecular gas emission in the Milky Way show that while the cloud mass spectrum extends over several orders of magnitude, a majority of the molecular gas mass is contained in large, massive cloud complexes, which are typically ~ 40 pc in diameter and have masses on the order of $1 \times 10^5 \ M_\odot$; these complexes are usually referred to as giant molecular clouds (GMCs)[1] and are considered to be the basic organizational unit of the molecular ISM (Scoville 1990; Combes 1991; Young & Scoville 1991).

Compared to the Milky Way, the properties of GMCs in external galaxies are not well known. The primary reason for this is a lack of high-resolution, high-sensitivity data, which are necessary for spatially resolving individual complexes. Only in the Magellanic Clouds can single-dish telescopes resolve extragalactic GMCs (Israel et al. 1993; Rubio et al. 1993; Fukui et al. 2001). Even in the nearest spirals (e.g., M31 or M33), the angular size of a typical 40 pc GMC is $\sim 12''$, approximately half the resolution of the IRAM 30 m single-dish telescope at 2.6 mm, the wavelength of the CO($J = 1$–0) line emission. For these galaxies, interferometric observations are necessary to resolve GMCs.

GMCs have been detected using millimeter interferometers in the two nearest spiral galaxies, M33 (Wilson & Scoville 1990; Engargiola et al. 2003; Rosolowsky et al. 2007) and M31 (Vogel et al. 1987; Wilson & Rudolph 1993; Loinard & Allen 1998; Rosolowsky 2007). In M33, Wilson & Scoville (1990) observed 19 different fields and identified over 30 GMCs, but only 9 GMCs were suitable for a study of cloud properties. The number of GMCs detected in most spiral galaxies has been less than a dozen, presumably due to the small coverage area. This is beginning to change. Recently, a survey of M33 was undertaken by the BIMA (Berkeley-Illinois-Maryland Association)[2] array. The angular resolution was coarse ($\sim 13''$) but adequate to identify nearly 150 GMCs (Engargiola et al. 2003; see also Rosolowsky et al. 2007). With the

---

[1] In this paper we use the terms "giant molecular clouds," "GMCs," and "cloud complexes" interchangeably.

[2] The BIMA array was partially funded by grant AST 99-81289 from the National Science Foundation.

upcoming CARMA telescope, groundbreaking studies like the M33 survey are likely to become routine for external galaxies.

It is important to note that previous studies of GMCs in external galaxies have used different instruments with varying angular and linear resolutions and sensitivity. Moreover, these studies have used different cloud identification methods to define GMCs and determine their properties. Yet, in almost all of these studies, the observations have detected discrete molecular features similar to Galactic GMCs. Particularly notable is the consistent line width–size relationship in most of these observations.

However, several studies have noted differences between Galactic GMCs and those found in some irregular and dwarf galaxies. In the irregular galaxy NGC 6822 (Wilson 1994) and the SMC (Rubio et al. 1993), the clouds are slightly less massive and perhaps smaller than clouds seen in the Milky Way. In the LMC, Cohen et al. (1988) find that for a given size and line width, the clouds are about 6 times fainter in CO than comparable clouds in the Milky Way. The same is true of the dwarf NGC 1569, where the CO-to-H_2 conversion factor is reported to be 6 times larger than the Galactic value (Taylor et al. 1998). In IC 10, the cloud sizes and masses are similar to the Milky Way clouds, but the CO-to-H_2 conversion factor may be twice as high as that seen in the Galaxy if the clouds are assumed to be self-gravitating (Wilson & Reid 1991). These studies suggest that there are noticeable differences between the Galactic GMCs and those found in irregular or dwarf galaxies that may be attributed to the different host environments (e.g., metallicity) of these galaxies.

GMCs in the three nearest spiral galaxies, M31, M33, and the Milky Way, can be observed at sufficiently high resolution ($\sim$20 pc) to remove ambiguities from coarse resolution. Are the GMC properties in these spiral galaxies fundamentally different? Wilson & Scoville (1990) claim that no GMC larger than $4 \times 10^5 \, M_\odot$ is seen in M33, and unlike the Milky Way, 50% of the molecular mass in M33 resides in small clouds with masses less than $8 \times 10^4 \, M_\odot$, based on a comparison of interferometric and single-dish flux from the CO($J = 1-0$) line. On the other hand, analysis of the $^{13}CO/^{12}CO$ line ratio for a number of M33 clouds suggests that the total mass measured from the $^{12}CO(J = 1-0)$ line may be overestimated and the actual conversion factor from the CO-to-H_2 mass may be lower in the diffuse gas; in that case, the amount of mass in GMCs would constitute most of the molecular mass in M33 (Wilson & Walker 1994). With coarser resolution data, Engargiola et al. (2003) find a steep GMC mass spectrum in M33 and report a characteristic mass of $7 \times 10^4 \, M_\odot$. They conclude that molecular clouds in M33 are formed rapidly from the atomic gas and are short-lived entities.

On the other hand, in M31 Vogel et al. (1987) and Wilson & Rudolph (1993) noted that the four GMCs they detected were similar to Galactic GMCs. Loinard et al. (1999) smoothed a section of the Carina arm in the Milky Way to the resolution of single-dish M31 maps and concluded that there are general similarities between the distribution of molecular gas in M31 and the Milky Way. Similar results were also found by Heyer et al. (2000), who compared the molecular gas in M31 and the Milky Way using single-dish observations. In their study, Heyer et al. (2000) found a number of similarities in the molecular gas properties between M31 and the Milky Way, such as the amount of molecular gas at radii larger than 8 kpc, large arm-to-interarm contrasts, and similar surface brightnesses, line widths, and spacings of GMCs in spiral arms. Rosolowsky (2007) recently completed a large survey of clouds in M31. He also found that the GMCs in M31 are similar to those found in the Milky Way. These results depend on comparison of properties derived from data sets which are obtained with a different instrument and analyzed with different methods of cloud identification. The Milky Way data, for example, come from single-dish observations with a signal-to-noise ratio that is at least 2–4 times higher than in the M33 and M31 data sets. The data sets also differ in that single-dish telescopes are inherently different from the aperture synthesis maps: the interferometer will miss smooth, extended emission, whereas the single-dish data may suffer from beam dilution. The Milky Way survey also suffers from varying linear resolution. Finally, the methods for identifying clouds in the different Milky Way studies vary. These studies (e.g., Dame et al. 1986; Sanders et al. 1985) have usually projected a typical (l, b, v) cube onto one of its axes and used an integrated intensity contour to identify discrete features they call "clouds" or "complexes." The sizes were measured from the total area of the cloud, assuming that the cloud was spherical (Dame et al. 1986), or by measuring the chord across the velocity centroid in a position-velocity diagram (Sanders et al. 1985). In M33, Wilson & Scoville (1990) used a two-tiered selection criterion which required that a cloud be 3 σ or more in two adjacent channels and that its summed flux be at least 3 σ above the noise.

The lack of consistency in these methods and differences in observing techniques are worrisome. A proper comparative study of GMCs in these galaxies requires that the differences described above be eliminated. This is particularly important in view of future telescopes such as CARMA and ALMA, which will have the ability to mosaic large regions of galaxies like M31 and M33. The large-scale surveys will have the detail necessary for in-depth comparisons of the molecular ISM in Local Group and more distant galaxies. These future studies will address the fundamental question of how the molecular ISM varies from galaxy to galaxy. Knowing this is critical to understanding star formation and galaxy evolution.

In this paper we make an attempt to do a fair comparison of molecular emission in the three nearest spiral galaxies, i.e., M31, the Milky Way, and M33. We compare the M31 complexes to the simulated Milky Way complexes and previous surveys, using a cloud identification technique in which we identify complexes using a single integrated intensity contour (§ 3), and discuss how previous conclusions about M33 would change if the same technique of cloud identification were used (§ 4.1). An important addition to this analysis would be the addition of single-dish data for the M31 and M33 clouds, which would allow for an even more comprehensive comparison. Of course, one would still need to project the Milky Way clouds to the distance of Andromeda to compare the clouds at the same spatial resolution. Our method is intended to lay the groundwork for future studies that will compare molecular clouds across galactic environments and different galaxy types with telescopes such as CARMA, SMA, and ALMA.

In § 4.2 we describe two automated cloud identification algorithms (Gaussclump, developed by Stutzki & Güsten [1990], and Clumpfind, developed by Williams et al. [1994]) and their advantages and disadvantages. While we do not advocate using these algorithms to describe the characteristics of GMC populations in a galaxy, these algorithms may be used to compare the M31, M33, and simulated Milky Way data. We describe the results of this experiment in § 4.3 and discuss our overall conclusions in § 5. Preliminary results from this work have been published in Sheth et al. (2000).

2. OBSERVATIONS

2.1. *M31 BIMA Observations*

We observed CO($J = 1-0$) emission in the northeastern spiral arm of M31 with the BIMA array. Using a seven-pointing hexagonal grid (one central pointing surrounded by a ring of six pointings, each separated by 53$''$ from its two neighbors in the ring

Parameter	Value
α (J2000.0)[a]	$00^h45^m07.57^s$
δ (J2000.0)[a]	$41°35'46.68''$
V_{LSR}	-135 km s^{-1}
Total bandwidth	142.85 km s^{-1}
Velocity resolution	0.254[b] km s^{-1}
Projected baselines..	2.2–30.2 kλ
Single-sideband T_{sys}	275–1000 K
Calibration quasar	0136+478
Absolute flux calibrator	Uranus
Typical uncertainty in flux calibration	15%
Beam	$7.11'' \times 5.71'' \times 4.7°$
Noise in 2.6 km s^{-1} channel................................	0.15 Jy beam^{-1}

[a] Central pointing.
[b] Correlator data taken at 0.254 km s^{-1} resolution. Data were later smoothed to 2.6 km s^{-1} resolution for imaging.

and the center), we mosaicked a region known to have strong single-dish CO emission (point 4,0 in Ryden & Stark 1986). The mosaicked fields were observed sequentially with an integration time of 1 minute per field for 35 minutes, at the end of which the calibrator was observed for 3 minutes. The total data presented here were collected in five separate tracks for a total integration time of 18.2 hr, or 2.6 hr per field. The fields were combined using MIRIAD (Sault et al. 1995) with an algorithm developed by Sault et al. (1996). Note that the final maps generated from this algorithm have variable gain and sensitivity. The noise increases monotonically from the map center toward the edge. The gain is constant over a fairly large region (in this case, the central $\sim180''$) and then drops sharply to the edge. For our analysis, we only considered the region where the gain was higher than 0.4. Further details of the observations are given in Table 1.

2.2. M33 and Milky Way Data

The M33 survey was conducted by Wilson & Scoville (1990) with the OVRO (Owens Valley Radio Observatory)[3] millimeter array. The data reduction process is described in Wilson & Scoville (1990).

The Milky Way observations and reductions are from the 1.2 m CfA survey (Dame et al. 2001). The different complexes studied in the present work have been previously published as follows: Gem OB1 (Stacy & Thaddeus 1991), W3CO (Digel et al. 1996), Cas A (Ungerechts et al. 2000), and the Carina arm (Grabelsky et al. 1987; Bronfman et al. 1989). Table 2 lists the data sets and instruments used in this study.

3. RESULTS: M31 CLOUDS

In Figure 1 we show the velocity-integrated CO($J = 1-0$) intensity map in contours overlaid on a gray-scale optical[4] image. Our field of view encompasses two dust lanes, which can be seen trending diagonally across the field from northeast to southwest. The majority of the CO emission lies in these two dust lanes, which are separated by a distance of 2 kpc (assuming an inclination $i = 77°$). There are six distinct molecular cloud complexes, which are labeled A–F. The complex labeled E lies along a dust spur which runs between the two dust lanes. We rotated the data cube, collapsed one spatial dimension, and generated right ascension–velocity and declination-velocity maps for each complex. We checked these maps to verify that each complex is a well-defined and separate entity. None of the complexes have emission separated by more than a few kilometers per second, except complex C.

In Figure 2 we show channel maps in which CO($J = 1-0$) emission is detected. These maps highlight the complex structure present in these clouds. Complex A, toward the northern edge of our field of view, is in the dust lane adjacent to a bright H II region. Further south in the dust lane is complex B, which has considerable structure; it is made up of at least two or three different clumps which the automated algorithms separate into different clumps. Complex C is the weakest complex in our maps. It is patchy and extends over a large region and over 10 km s^{-1} in velocity. The spectrum for this complex shows that it may be a blend of several clouds. Therefore, we do not calculate the size or velocity width for this complex. Complex D may be considered a prototypical GMC; it is well isolated, i.e., unblended, and has nice symmetry. This complex is also rather weak, but we are fortunate that it is near the center of our mosaicked field where the noise is the lowest in these maps. Complex E lies along the dust spur connecting the two dust lanes and also has considerable structure. There are at least two or three peaks of emission in this complex. Complex F is an elongated complex toward the western edge of our field of view; this is the brightest complex in our field of view. We also show the boxes used to extract the spectrum and sum the emission for each complex. From these, we calculated the virial and molecular mass for each complex. The properties thus derived are listed in Table 3. The method used for identifying these clouds is discussed in the next section.

4. COMPARING CLOUDS WITH DIFFERENT CLOUD IDENTIFICATION ALGORITHMS

4.1. The Integrated Intensity Contour Method

We used a specified integrated intensity contour (2 K km s^{-1}) to define a complex. Is this justified, especially when many of

TABLE 2
Data Sets and Instruments

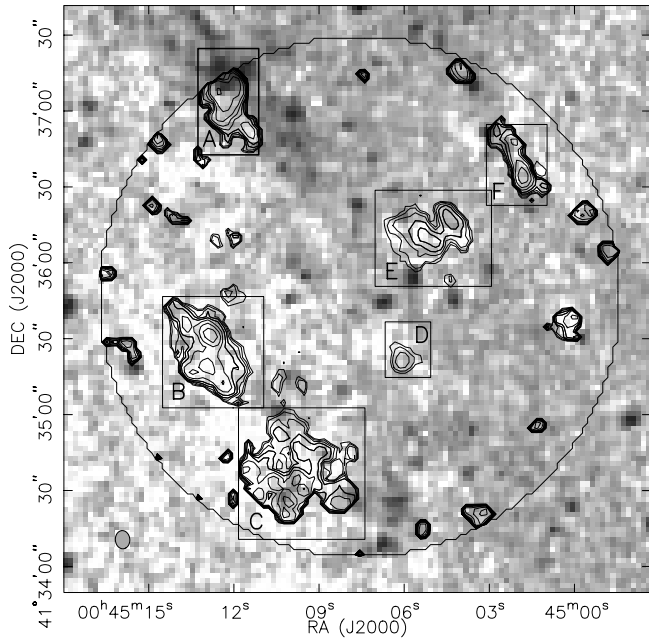| Galaxy	Observatory	Angular/Linear Resolution	Assumed Distance (kpc)
M31	BIMA	$7.11'' \times 5.71''$/19–24 pc	690
M33	OVRO	$5''-7''$/19–26 pc	790
GEM OB1 (Milky Way)	CfA 1.2 m	8.8'/5.1 pc	2
Cas A (Milky Way)..........................	CfA 1.2 m	8.8'/5.1 pc	2
W3CO (Milky Way)........................	CfA 1.2 m	8.8'/6.4 pc	2.5
Carina[a] (Milky Way)........................	CfA 1.2 m	8.8'/34.8 pc	13.6

[a] Carina data not used in comparative study.

Fig. 1.— Velocity-integrated, primary beam–corrected intensity map of the M31 field shown in logarithmic contours of $1.5^n \times 2$ K km s^{-1}, where $n = -1$, 1, 2, 3, ... The gray-scale image is a DSS J-band image in reverse color, so that white represents obscuring dust. The six complexes used for comparison to the Milky Way are identified with the boxes labeled A–F. The outer circle is the gain = 0.4 contour.

these complexes clearly have substructure? From our experience with previous Milky Way studies, we believe that any cloud complex can always be divided and subdivided into smaller and smaller clouds because the molecular medium is extremely clumpy with a low volume filling factor (see, e.g., Dame et al. 2001). The higher the resolution, the more likely it is that a given structure may be divided into smaller components. Having said that, however, a complex has definite boundaries. Therefore, the integrated intensity contour in a collapsed cube (i.e., collapsed along one axis) seems to be a reasonable way of identifying a molecular cloud complex and evaluating its properties. This has been applied to GMC studies in the Milky Way (e.g., Sanders et al. 1985). Thus, we can compare M31 clouds directly to the previous Milky Way studies. As a check on the method, we applied it to a few Milky Way complexes (Gem OB1, W3CO, and Cas A) and to a few complexes in M33. We projected the Milky Way clouds to the distance of M31 and simulated their interferometric observation using the same u-v tracks actually obtained for the BIMA observations of M31. The details of these simulations are in the Appendix. Using this approach, each of the three Milky Way complexes was decomposed into two clouds. We refer to the Milky Way complexes projected to the distance of M31 and observed with the interferometer as "simulated" clouds for the remainder of this paper; the reader should keep in mind that these clouds are not artificial but are actual Milky Way clouds which are being "observed" as if they were in Andromeda and were observed with BIMA. The properties of the complexes thus defined are listed in Table 4.

When we compare the properties of the complexes we observe in M31 to those observed previously in the Milky Way (e.g., Dame et al. 1986; Sanders et al. 1985), we find that the mean properties of the complexes in the two galaxies are not significantly different. Whereas Dame et al. (1986) found complexes ranging from 24 to 262 pc in diameter with velocity widths of 4–18 km s^{-1}, the com-

plexes in M31 range from 40 to 75 pc and 4.7–7.8 km s^{-1}. In Figure 3 we place our M31 complexes, the Milky Way clouds from Dame et al. (1986), and a set of simulated Milky Way clouds on the size–line width plot from Dame et al. (1986). The Dame et al. (1986) GMCs are particularly useful for this figure because they have a larger dynamic range in size and line width than the other sets of clouds. Within the errors, the M31 complexes fall along the same relationship found in the much more extensive Milky Way survey. It is also worth noting that the Milky Way GMCs simulated at the distance of Andromeda and observed with an interferometer show line widths and sizes that are also consistent with the standard relationship. The main point of this figure is that data for different galaxies, whether observed with a single-dish telescope or an interferometer, can be compared equivalently so long as the observations have comparable spatial resolution (i.e., the observations sample the same spatial scales in different galaxies) and sensitivity and the data are analyzed with the same cloud identification technique(s).

For identifying clouds in M33, Wilson & Scoville (1990) did not use the same cloud identification method as described above. In their method, if a cloud could be resolved by eye in a channel and separated spatially or in velocity from an adjacent cloud, then the cloud was considered to be a distinct cloud. The effect of this technique is similar to that of the automated algorithms such as Clumpfind[5] and Gaussclump, which we discuss in more detail in § 4.2. Basically, the Wilson & Scoville (1990) method breaks apart complexes whenever possible. Thus, it was difficult to deduce from their analysis whether the M33 clouds are indeed a different population than the Milky Way clouds.

We reanalyzed Figure 2 from Wilson & Scoville (1990) using the integrated intensity contour method and found that several of the M33 clouds merged into larger complexes. The main reason for that is that the lowest contour shown in Figure 2a of Wilson & Scoville (1990) is 7 K km s^{-1}, a very high emission level. When we use a 2 K km s^{-1} contour, clouds MC-6, MC-7, and MC-8 in field 4C become one complex with a total molecular mass of 4.3×10^5 $M_\odot$. Similarly, in field 4B clouds 11 and 12 ($M_{tot} = 2.4 \times 10^5$ $M_\odot$) and in field 2C clouds 16 and 17 ($M_{tot} = 2.1 \times 10^5$ $M_\odot$) become single complexes. Also, all the clouds (except cloud 3, which is at a very different velocity) in field 1A merge into one complex. With better sensitivity, clouds 1, 2, 4, and 5 might be seen as belonging to one complex which would have a total mass of at least 4.9×10^5 $M_\odot$. Although the difference in the mass of the merged clouds is not significant, the earlier conclusion that no cloud larger than 4×10^5 $M_\odot$ exists in M33 appears to be due to a different choice in cloud identification method and the low sensitivity of the observations. Our analysis is intended to show the need for using the same cloud identification and analysis technique for comparing cloud properties.

In summary, although we only have a handful of clouds to compare with the Milky Way, we find that the M31 and M33 GMCs are similar in most respects to those found in the Milky Way. The small number of clouds prevents us from studying the mass function of GMCs in M31.

4.2. Automated Clump-Finding Algorithms

Automated algorithms such as Clumpfind (Williams et al. 1994) and Gaussclump (Stutzki & Güsten 1990) work on the opposite

---

[5] In fact, when we used Clumpfind on the Wilson & Scoville data, we found every one of their clouds, but Clumpfind actually merged four pairs of these clouds into a single cloud.
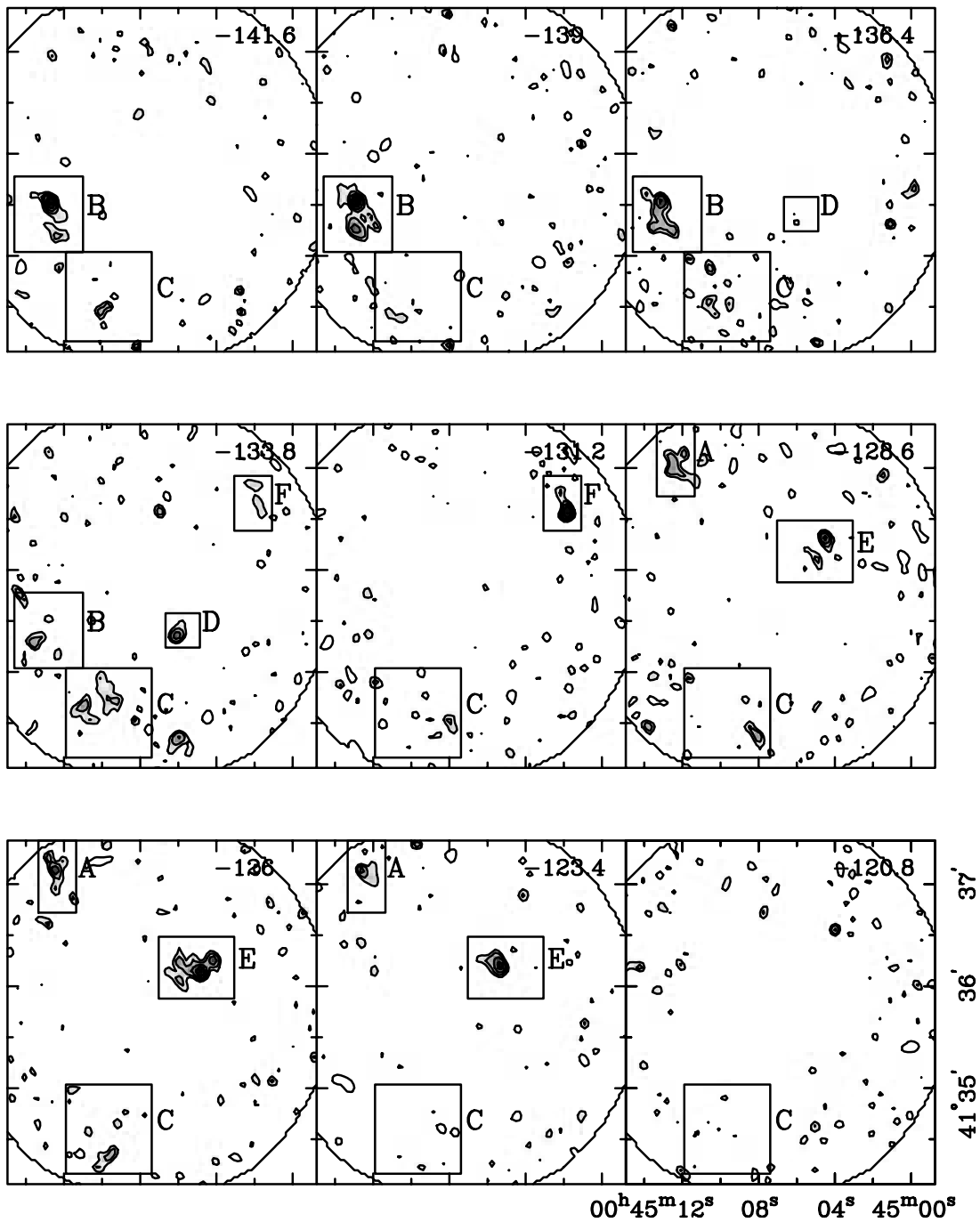
Fig. 2.— Channel maps showing the CO($J = 1-0$) emission in the northeastern spiral arm of M31. These maps are not primary beam–corrected. The contours are logarithmic, $1.5^n \times 0.22$ Jy beam^{-1}. The boxes show the complexes A–F. The channel maps are 2.6 km s^{-1} wide starting at -142 km s^{-1}. The outer circle is the gain = 0.4 contour.

TABLE 3
Properties of M31 GMCs

Cloud	R.A. (J2000.0)	Decl. (J2000.0)	V_{peak} (km s^{-1})	V_{FWHM}[a,b] (km s^{-1})	T_B^{*}[c] (K)	S_{CO}[a] (Jy km s^{-1})	Diameter[a,d] (pc)	M_{vir}[a,e] ($\times 10^5 M_\odot$)	M_{mol}[a,f] ($\times 10^5 M_\odot$)
A...............	00 45 12.42	41 37 07.23	−126	7.8	3.32	40.8	44.5	2.68	3.13
B...............	00 45 12.73	41 35 24.49	−139	7.8	3.61	67.6	71.2	4.29	5.18
C...............	00 45 08.69	41 27 49.58	−134	...	1.57	...	...	...	...
D...............	00 45 06.04	41 35 23.25	−134	4.7	2.02	11.1	41.1	0.89	0.85
E...............	00 45 04.97	41 36 11.69	−126	6.2	3.34	55.4	73.6	2.80	4.25
F	00 45 01.96	41 36 38.99	−131	6.2	4.24	23.6	57.4	2.2	1.80

Note.—Units of right ascension are hours, minutes, and seconds, and units of declination are degrees, arcminutes, and arcseconds.
[a] Typical errors are: D, ±4 pc; V_{FWHM}, ±1.3 km s^{-1}; S_{CO}, ±20%; M_{vir}, ±30%; and M_{mol}, ±30%.
[b] Full width at half-maximum measured from the spectrum.
[c] Brightest pixel in channel maps.
[d] Average of deconvolved major and minor axis Gaussian fit to integrated intensity map of complex.
[e] $M_{vir} = 99 \times V_{FWHM}^2 \times$ diameter.
[f] $M_{mol} = (1.61 \times 10^4) d^2 S_{CO}$. This assumes a Galactic value for the conversion factor between the CO flux and the hydrogen column density of 3×10^{20} cm^{-2} (K km s^{-1})$^{-1}$ and includes a factor of 1.36 to account for helium and other heavy elements.

philosophy from the single contouring algorithm described above: both Clumpfind and Gaussclump break apart a complex into as many parts as possible. Clumpfind contours the cube into discrete intervals specified by the user. Then it works its way through the contouring levels identifying isolated peaks as possible individual clumps. Clumpfind then assigns all pixels above the lowest contouring interval to one or the other clump. Finally, it merges clumps which are closer than the spatial or velocity resolution. The advantage of this algorithm is that it has no preconceptions of the shape of the clouds and hence readily deals with the complex structure of GMCs. On the other hand, the contouring technique tends to clip away too many pixels, which can lead to incorrect calculation of sizes and line widths. This may be particularly problematic for data cubes with low dynamic range. Gaussclump avoids such problems of noisy or low dynamic range data by directly fitting clouds in the data cube. It tries to fit peaks of emission with an 11 parameter Gaussian, also taking into account the resolution of the observations. The biggest disadvantage of this method is that it is restricted to defining clumps as Gaussian, which is seldom the shape of the observed molecular emission.

Neither method is particularly well-suited to analyzing GMC properties. The reason has more to do with molecular clouds than the algorithms themselves. Molecular cloud structure is extremely complex, at least as observed in the Milky Way. These algorithms tend to divide a complex into as many subdivisions as allowed by the resolution of the data. Hence, these methods seldom find structures which are larger than one or two resolution elements. For example, if the resolution of a survey is 5 pc, these methods will not find a 100 pc complex, because peaks of emission located more than 5 pc apart will be classified as separate clouds. The bias thus introduced is not fatal because cloud/clump properties in equivalent data sets (i.e., data sets with similar resolutions and noise characteristics) may still be compared, but generalizations about a galaxy's cloud population cannot be drawn. This is especially pertinent to extragalactic astronomy, where higher and higher resolution observations are continually being achieved with improvements in millimeter-wave interferometry.

We advocate that since molecular clouds generally have fairly sharp edges, the simplest cloud identification algorithm is the integrated intensity contouring method, where one identifies the contour level associated with the edge of the cloud (e.g., Sanders et al. 1985; Dame et al. 1986) in a three-dimensional cube. The obvious shortcoming of this method is that it ignores the structure in the clouds. Another obvious disadvantage of the method is that it is difficult to automate and is quite time-consuming because one has to make three different moment maps along the different axes and decide what the distinct complexes are. This method may suffer from blended emission, but this confusion will be limited in extragalactic sources. Rosolowsky & Leroy (2006) have recently introduced a new method for identifying and analyzing molecular clouds

TABLE 4
Properties of Milky Way GMCs Simulated at M31

Cloud	V_{FWHM}[a,b] (km s^{-1})	T_B^{*}[c] (K)	S_{CO}[a] (Jy km s^{-1})	Diameter[a,d] (pc)	M_{vir}[a,e] ($\times 10^5 M_\odot$)	M_{mol}[a,f] ($\times 10^5 M_\odot$)
Gem1....................................	7.2	4.0	70.87	66.0	3.4	5.4
Gem2....................................	11.1	2.9	105.4	98.2	12.0	8.0
W1..	9.9	2.4	42.62	40.1	3.9	3.3
W2..	5.5	1.3	22.21	61.5	1.8	1.7
CasA1....................................	7.7	4.5	260.9	123.0	7.2	20
CasA2....................................	10.6	2.9	81.8	62.5	6.9	6.3

[a] Typical errors are: D, ±4 pc; V_{FWHM}, ±1.3 km s^{-1}; S_{CO}, ±20%; M_{vir}, ±30%; and M_{mol}, ±30%.
[b] Full width at half-maximum measured from the spectrum.
[c] Brightest pixel in channel maps.
[d] Average of deconvolved major and minor axis Gaussian fit to integrated intensity map of complex.
[e] $M_{vir} = 99 \times V_{FWHM}^2 \times$ diameter.
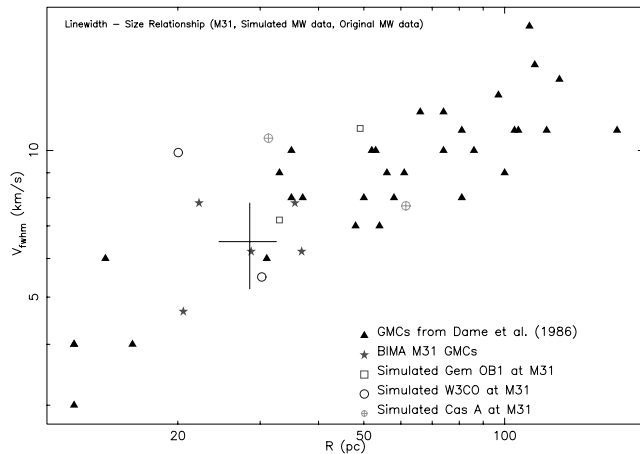[f] $M_{mol} = (1.61 \times 10^4) d^2 S_{CO}$.

Fig. 3.—Size–line width relationship for the M31 complexes (*stars*), simulated Milky Way GMCs (*squares, circles, circled plus signs*), and previously analyzed Milky Way complexes (*triangles*) by Dame et al. (1986). The typical error in measurements of the velocity width and radius are shown with a cross at the mean value of the M31 clouds in the survey. All the data points fall on the line width–size relationship defined by the Dame et al. (1986) Milky Way data. The data, whether from a single-dish telescope or an interferometer, give equivalent results when the observations sample the same spatial scales and have comparable sensitivities in different galaxies. [*See the electronic edition of the Journal for a color version of this figure.*]

which may avoid many of the biases inherent in other methods discussed above; this method may be a useful tool for future surveys of molecular clouds in nearby spirals with CARMA and ALMA.

4.3. *M31, M33, and Milky Way Cloud Properties Using Gaussclump*

We ran Gaussclump on all CO data sets in all three galaxies. We found 17 clouds in our BIMA M31 survey, 35 clouds in the M33 survey of Wilson & Scoville (1990), 7 clouds in the simulated Gem OB1 complex, 5 clouds in the W3CO complex, and 13 clouds in the Cas A complex. These results should be compared to the six complexes found in M31 and the two complexes found in each of the simulated Milky Way clouds using the integrated intensity contouring method. The mean values for the amplitudes, velocity widths, and sizes are listed in Table 5. The velocity widths and sizes have not been deconvolved. Note that the M33 clouds were not simulated at the distance of M31 and observed with BIMA. These data are similar to M31, but many fields have a slightly coarser resolution ($8''$–$9''$) than the BIMA data.

The derived properties are also shown graphically in Figure 4. The plots show no significant differences in the amplitudes, sizes, or velocity widths for the three galaxies. We plot each of the de-

rived properties against another derived property to test whether there is any dependence of one on the other, and find none.

Our conclusion from this experiment is similar to that derived from the analysis of the integrated intensity contouring method. The molecular clouds in these data sets, when compared in a consistent manner, show no significant differences.

5. CONCLUSIONS

In the northeastern spiral arm of M31, we have identified six distinct, large complexes of molecular gas. All of these complexes lie along the spiral arm dust lanes or, in one case (complex E), along a dust spur between the dust lanes. These complexes have a mean diameter of 57 ± 13 pc, a mean velocity width of 6.5 ± 1.2 km s^{-1}, and a mean molecular mass of $(3.0 \pm 1.6) \times 10^5$ $M_\odot$ and are indistinguishable from those found in the Milky Way, e.g., Dame et al. (1986).

Meaningful comparison of GMCs in different galaxies requires consistent analysis of data taken with different instruments and different cloud identification techniques. This paper represents an attempt at eliminating such differences and comparing GMCs in M31, M33, and the Milky Way in as consistent a manner as possible. We have simulated three Milky Way complexes at the distance of M31 and observed them with the BIMA array. The simulations show that interferometers are excellent at recovering molecular complexes in the Local Group galaxies. We compared the simulated Milky Way complexes to the M31 data using an integrated intensity contour method and found that the complexes thus identified and analyzed fell within the same line width–size relationship as found by Dame et al. (1986). The M33 clouds, if analyzed in this manner, also yield larger clouds than previously stated. Larger interferometric surveys of these galaxies are necessary to compare the GMC distribution and mass function to that in the Milky Way (e.g., Engargiola et al. 2003; Rosolowsky 2007).

Finally, we compared two automated algorithms, Clumpfind and Gaussclump, and found that Gaussclump was better at recovering cloud properties than Clumpfind for low dynamic range data. Our experiments revealed that such algorithms are resolution-dependent and that the inherent clumpy nature of molecular emission prevents these methods from identifying clouds larger than one or two resolution elements. Hence, we caution against using these methods to characterize GMC populations in galaxies. Still, these may be used to quickly compare properties of clouds in data with similar noise and resolution characteristics. Using Gaussclump, we find that the cloud properties in M31, M33, and simulated Milky Way data are indistinguishable.

TABLE 5
Mean of Gaussclump Derived Properties

Galaxy	Number of Clouds	Amplitude (Jy beam^{-1})	$V_{\rm FWHM}$ (km s^{-1})	Size (arcsec)
M31	17	0.9 ± 0.4	3.6 ± 1.0	7.4 ± 1.3
M33	35	0.9 ± 0.3	4.9 ± 1.7	8.4 ± 1.4
Gem OB1[a]	7	1.0 ± 0.4	4.3 ± 0.7	8.4 ± 1.1
W3CO[a]	5	0.6 ± 0.2	4.7 ± 1.3	7.6 ± 1.3
Cas A[a]	13	1.0 ± 0.4	5.3 ± 1.5	8.8 ± 1.8

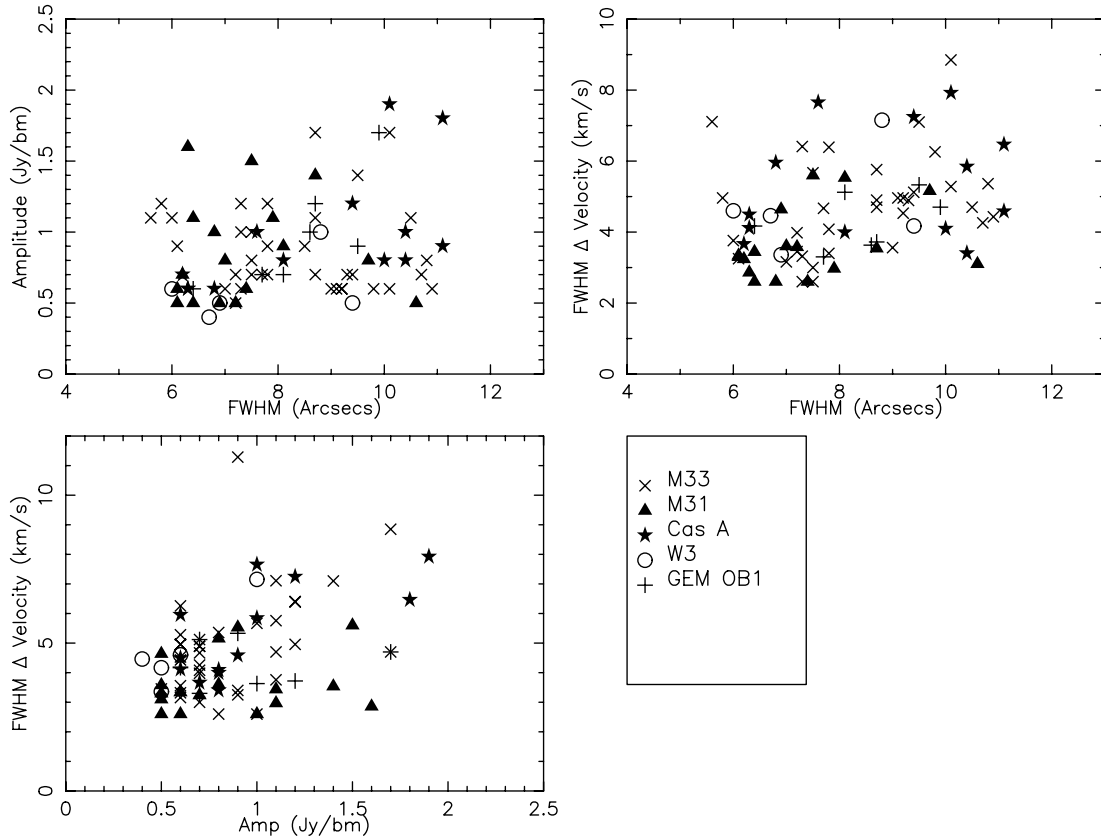[a] These values refer to the simulated Milky Way clouds at the distance of M31.

FIG. 4.— Three derived properties compared with each other for each of the data sets: M31, M33, and the simulated Milky Way clouds Cas A, Gem OB1, and W3CO. No attempt has been made to deconvolve the line widths or radii because all data sets have the same line widths and approximately the same angular resolution. The sizes are in arcseconds, line widths in kilometers per second, and amplitude in janskys per beam. There is no significant difference in the properties of the clouds identified by Gaussclump. The largest M33 clouds are the least affected by the coarse ($\sim 9''$) resolution. The cluster of small M31 clouds with low line widths are those in complex C. These are very weak clouds, and their properties are not well defined.

APPENDIX

A1. SIMULATION OF THE BIMA OBSERVATION OF MILKY WAY GMCs AT THE DISTANCE OF M31

The first step is to simulate the appearance of the Milky Way clouds if they were located at the distance of Andromeda. In other words, we needed to scale the Milky Way maps to the distance of M31, which we did by scaling the map header values for the angular size of the map pixels by the ratio of the distance to each Milky Way complex to that of M31. The next step is to simulate observation of the distance-scaled Milky Way data with the BIMA interferometer. To get a precise match in the point-spread function, we modified the header values for the right ascension and declination at the field center so as to match the position of the BIMA M31 observation; this enabled the u-v tracks for the simulated observations to match the actual observations. The original temperature scale, which was in units of T_A^*, was converted to janskys per beam, and the maps were gridded to a $2''$ pixel scale. A separate model was then created for each mosaicked pointing; each model had a primary beam taper applied to it. All seven of these models were then observed with the u-v tracks used for M31. Since the original Milky Way data were approximately half as noisy as the BIMA data, we simulated additive noise in the u-v plane and added that to our final maps. The final simulated Milky Way maps are therefore reflective of the effects of spatial filtering by the interferometer and are similar in almost every way to the M31 and M33 data.

A2. EFFECT OF INTERFEROMETRIC FILTERING ON SIMULATIONS OF MILKY WAY OBSERVATIONS

We initially began this comparative study project with a section of the Carina arm from the 1.2 m survey because, at a heliocentric distance of 13.6 kpc, the Milky Way survey's linear resolution matched the BIMA observations of M31. However, when we simulated the Carina clouds, the simulated maps showed significant differences, as displayed in Figure 5. The bottom panels of this figure show a single velocity channel from the Carina simulations. The first column of panels is the model Carina complex at the distance of M31 before BIMA observations. The second column is the model after BIMA observations, i.e., the simulated map. Both of these
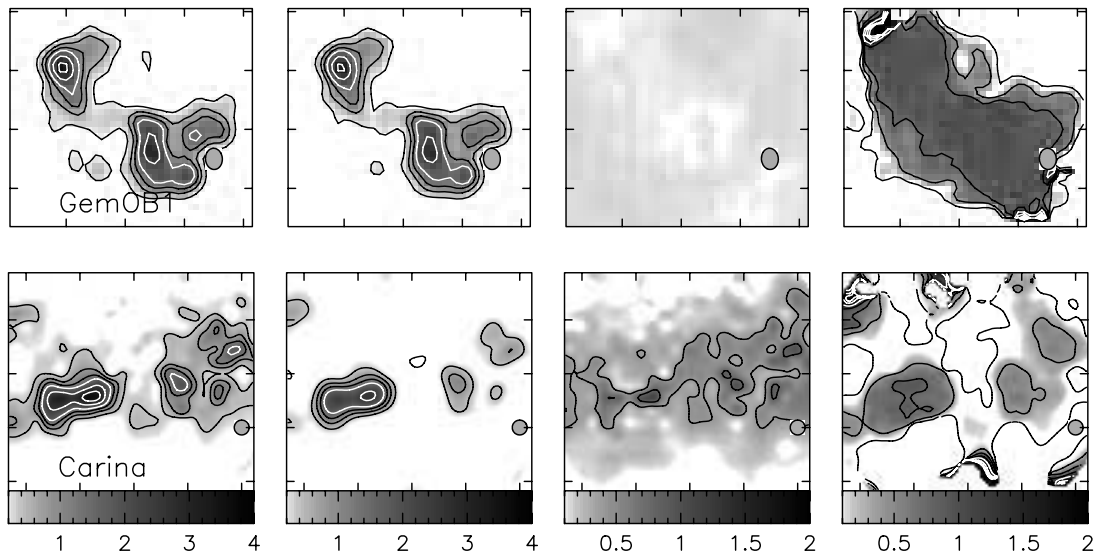
Fig. 5.—*Top panels*, channel from the simulation of the Gem OB1 complex; *bottom panels*, channel from the simulation of the Carina complex. The first column of panels shows the Milky Way cloud at the distance of M31. The second column shows the cloud simulated with interferometric observations with BIMA. The gray-scale wedge in the bottom panels is an indication of the flux in janskys per beam for the first three columns; it is a ratio for the fourth column. In the second column one can immediately note that the Carina cloud is significantly dimmer than its input model, whereas the Gem OB1 cloud appears unchanged. The third column shows the model cloud minus the simulated image, and the fourth column shows the simulated image divided by the model image. The third column is in janskys per beam. Notice that almost no flux is lost in the Gem OB1 simulation, whereas the Carina arm cloud is weaker by as much as 30%–50%.

columns are on the same gray scale and have the same contour levels. The third column of panels is the input model minus the simulated map, and the fourth column is the simulated map divided by the input model. One immediately sees the reduction in the flux in these maps. The clouds are dimmer by a factor of 30%–50%. The flux that is resolved out is not a uniform background but rather structure on all scales. We further tested these effects by changing the orientation of the Carina model clouds by shifting them in different directions and rotating them at various angles. In every case, we saw the same result: the flux was reduced by as much as 50%.

When we repeated the experiments for the Cas A, W3CO, and Gem OB1 clouds from the same Milky Way survey, we found a completely different result. The interferometer recovered almost all of the flux for these simulations. An example of this is shown in the top panels of Figure 5, which show a single velocity channel from the Gem OB1 simulations. The difference between the Carina clouds and these complexes is that these complexes are 4–6 times closer than Carina and were observed with a linear resolution of ∼5 pc compared to a resolution of ∼30 pc. The 1.2 m maps of the Carina clouds, therefore, have smoother emission on a larger scale than the Cas A, W3CO, and Gem OB1 clouds; this smooth emission is then subsequently resolved out by the interferometer. This filtering of flux from large, smooth structures by interferometers is expected and observed (e.g., Beck & Hoernes 1996; Helfer et al. 2002). Presumably, the Carina arm at higher resolution would look like the other Milky Way complexes we studied (Gem OB1, W3CO, and Cas A). Since the Carina arm model itself is incorrect, we cannot use the simulated Carina clouds in our comparative analysis. The recovery of the Gem OB1, W3CO, and Cas A clouds is reassuring because it means that interferometers are excellent at recovering the molecular emission in GMCs; this is due to the inherently clumpy nature of GMCs.

REFERENCES

Beck, R., & Hoernes, P. 1996, Nature, 379, 47
Blitz, L. 1993, in Protostars and Planets III, ed. E. H. Levy & J. I. Lunine (Tucson: Univ. Arizona Press), 125
Bronfman, L., Alvarez, H., Cohen, R. S., & Thaddeus, P. 1989, ApJS, 71, 481
Cohen, R. S., Dame, T. M., Garay, G., Montani, J., Rubio, M., & Thaddeus, P. 1988, ApJ, 331, L95
Combes, F. 1991, ARA&A, 29, 195
Dame, T. M., Elmegreen, B. G., Cohen, R. S., & Thaddeus, P. 1986, ApJ, 305, 892
Dame, T. M., Hartmann, D., & Thaddeus, P. 2001, ApJ, 547, 792
Digel, S. W., Lyder, D. A., Philbrick, A. J., Puche, D., & Thaddeus, P. 1996, ApJ, 458, 561
Engargiola, G., Plambeck, R., Rosolowsky, E., & Blitz, L. 2003, ApJS, 149, 343
Fukui, Y., Mizuno, N., Yamaguchi, R., Mizuno, A., & Onishi, T. 2001, PASJ, 53, L41
Grabelsky, D. A., Cohen, R. S., Bronfman, L., Thaddeus, P., & May, J. 1987, ApJ, 315, 122
Helfer, T. T., Vogel, S. N., Lugten, J. B., & Teuben, P. J. 2002, PASP, 114, 350
Heyer, H. M., Dame, T. M., & Thaddeus, P. 2000, in The Interstellar Medium in M31 and M33, ed. E. M. Berkhuijsen, R. Beck, & R. A. M. Walterbos (Bad Honnef: Shaker, Aachen), 29
Israel, F. P., et al. 1993, A&A, 276, 25

Loinard, L., & Allen, R. J. 1998, ApJ, 499, 227
Loinard, L., Dame, T. M., Heyer, M. H., Lequeux, J., & Thaddeus, P. 1999, A&A, 351, 1087
McGlynn, T., Scollick, K., & White, N. 1996, in IAU Symp. 179, New Horizons from Multi-Wavelength Sky Surveys, ed. B. J. McLean et al. (Dordrecht: Kluwer), 465
Rosolowsky, E. 2007, ApJ, 654, 240
Rosolowsky, E., Keto, E., Matsushita, S., & Willner, S. P. 2007, ApJ, 661, 830
Rosolowsky, E., & Leroy, A. 2006, PASP, 118, 590
Rubio, M., Lequeux, J., & Boulanger, F. 1993, A&A, 271, 9
Ryden, B. S., & Stark, A. A. 1986, ApJ, 305, 823
Sanders, D. B., Scoville, N. Z., & Solomon, P. M. 1985, ApJ, 289, 373
Sault, R. J., Staveley-Smith, L., & Brouw, W. N. 1996, A&AS, 120, 375
Sault, R. J., Teuben, P. J., & Wright, M. C. H. 1995, in ASP Conf. Ser. 77, Astronomical Data Analysis Software and Systems IV, ed. R. A. Shaw, H. E. Payne, & J. J. E. Hayes (San Francisco: ASP), 433
Scoville, N. Z. 1990, in The Evolution of the Interstellar Medium, ed. L. Blitz (San Francisco: ASP), 49
Scoville, N. Z., Yun, M. S., Sanders, D. B., Clemens, D. P., & Waller, W. H. 1987, ApJS, 63, 821
Sheth, K., Vogel, S. N., Wilson, C. D., & Dame, T. M. 2000, in The Interstellar Medium in M31 and M33, ed. E. M. Berkhuijsen, R. Beck, & R. A. M. Walterbos (Bad Honnef: Shaker, Aachen), 37

Stacy, J. A., & Thaddeus, P. 1991, in ASP Conf. Ser. 16, Atoms, Ions, and Molecules: New Results in Spectral Line Astrophysics, ed. A. D. Haschick & P. T. P. Ho (San Francisco: ASP), 197

Stutzki, J., & Güsten, R. 1990, ApJ, 356, 513

Taylor, C. L., Hüttemeister, S., Klein, U., & Greve, A. 1998, ApJ, 494, 581

Ungerechts, H., Umbanhowar, P., & Thaddeus, P. 2000, ApJ, 537, 221

Vogel, S. N., Boulanger, F., & Ball, R. 1987, ApJ, 321, L145

Williams, J. P., de Geus, E. J., & Blitz, L. 1994, ApJ, 428, 693

Wilson, C. D. 1994, ApJ, 434, L11

Wilson, C. D., & Reid, N. I. 1991, ApJ, 366, L11

Wilson, C. D., & Rudolph, A. L. 1993, ApJ, 406, 477

Wilson, C. D., & Scoville, N. 1990, ApJ, 363, 435

Wilson, C. D., & Walker, C. E. 1994, ApJ, 432, 148

Young, J. S., & Scoville, N. Z. 1991, ARA&A, 29, 581